

Colour symmetry and non-collinear altermagnetism

Paolo G. Radaelli

*Clarendon Laboratory, Department of Physics, University of Oxford, Oxford, OX1 3PU, United Kingdom**

Gautam Gurung

Trinity College, University of Oxford, Oxford, OX1 3BH, United Kingdom[†]

(Dated: January 7, 2025)

We present a formalism based on colour symmetry to analyse the momentum-space spin textures of non-collinear magnets. We show that, out of the spin textures allowed by the magnetic point group, one can extract an ‘altermagnetic’ component that is invariant by general rotations in spin space, and can exist in the absence of spin-orbit coupling. We demonstrate this approach in the case of three complex, non-collinear magnets, $\text{Mn}_3\text{Ir}(\text{Ge},\text{Si})$, Pb_2MnO_4 and Mn_3GaN . For Mn_3GaN , we also show that the predictions of colour-symmetry analysis are consistent with density functional theory calculations performed on the same system both with and without spin-orbit coupling.

I. INTRODUCTION

In the past five years, an intense theoretical and experimental effort has been focussed on magnetic systems having electronic bands with lifted spin degeneracy, particularly when this is not due to spin-orbit coupling (SOC) (for example Refs. 1 and 2 — see Ref. 3 for a full list of references). Materials displaying this phenomenology have been named ‘altermagnets’, though there is no complete consensus on the exact definition of this term. Two broad classes of magnetic materials are often included in this definition: altermagnets *stricto sensu*, in which spin splitting is $\mathbf{k}/-\mathbf{k}$ symmetric and time-reversal odd (TRO), and so-called *p*-wave magnets,⁴ in which spin splitting is $\mathbf{k}/-\mathbf{k}$ antisymmetric and time-reversal even (TRE). In analogy with the celebrated Rashba-Dresselhaus (R-D) effect,^{5,6} *p*-wave magnets require inversion-symmetry breaking, but unlike R-D systems, do not require SOC. In a previous paper³, one of us (PGR) presented a symmetry classification of $\mathbf{k}/-\mathbf{k}$ -symmetric, TRO splitting of electronic bands in magnetic materials based on a general tensorial approach. It was also shown that, for collinear antiferromagnets where the splitting is allowed, one can decompose the spin texture into two components: a SOC-independent ‘altermagnetic’ texture, having a general form that can be obtained via the spin-group SG analysis (or an analogue based on black-and-white Shubnikov groups), and a ‘residual’ component, which is allowed by the exact magnetic point group (MPG) symmetry for a particular direction of the Néel vector and will only exist in the presence of SOC. The existence of non-relativistic spin textures in *non-collinear* antiferromagnets has been discussed before the altermagnetism emerged as a distinct concept,⁷ with earlier observations dating as far back as 1989.⁸ Collinear and non-collinear magnets can possess the same MPG symmetries (though cubic MPG can only describe non-collinear magnets), and there is general consensus that the SG analysis, with some modifications, can be extended to non-collinear systems. Nevertheless, no systematic methods has been proposed to date to extract ‘altermagnetic’ textures in non-collinear systems. Here, we fill this gap by employing a systematic approach based on so-called colour symmetry groups (CG) to describe $\mathbf{k}/-\mathbf{k}$ symmetric, time-reversal odd altermagnetic textures in collinear and non-collinear magnets.⁹ CGs are a natural extension of black-and-white Shubnikov groups to cases in which there are more than two spin directions. In Ref. 3, it was shown that Shubnikov groups offer an alternative formulation of the SG analysis, and offer some advantages — for instance, they preserve the natural concept of time reversal symmetry. Here, we will also show that CGs and SGs are largely equivalent and can both be employed to describe non-collinear altermagnetic textures. However, CGs are more intuitive, and do not require the rather cumbersome choice of the SG axis orientation. We will demonstrate the application of this CG analysis to three non-collinear chiral magnets: $\text{Mn}_3\text{Ir}(\text{Ge},\text{Si})$, Pb_2MnO_4 and Mn_3GaN . The magnetic structures of $\text{Mn}_3\text{Ir}(\text{Ge},\text{Si})$ and Pb_2MnO_4 are described by complex four-colour symmetries, but do not break any crystal symmetries, which means that the CG and MPG analysis are expected to yield the same textures. Finally, we present CG analysis alongside spin-resolved density functional theory (DFT) calculations for the well-known non-collinear magnetic antiperovskite Mn_3GaN with and without SOC. We show that, in the absence of SOC, the spin texture is exactly as predicted by the CG analysis, while in the presence of SOC, an additional component emerges, which has the more general MPG symmetry and varies depending on the direction of the magnetic moments.

II. ALTERMAGNETISM AND SPIN-SPACE ROTATION INVARIANCE

The intuitive statement that the SOC-independent ‘altermagnetic’ component of the spin texture is invariant by rotation in spin space requires some qualification. In $\mathbf{k}/-\mathbf{k}$ symmetric TRO altermagnets, the spin texture can be described in terms of an effective Zeeman field $\mathbf{B}_i^{eff}(\mathbf{k}, m)$, which depends on the wavevector k and on the band index m .³ Within the tensorial framework, to a given order the effective Zeeman field can be expressed as

$$B_i^{eff}(\mathbf{k}, m) = T_{i,\alpha\beta\gamma\dots}^{(l)} k_\alpha k_\beta k_\gamma \dots \quad (1)$$

where $T_{i,\alpha\beta\gamma\dots}^{(l)}$ is tensor of odd rank that is symmetric in the Greek indices.

If \mathbf{B}_i^{eff} is generated by a collection of magnetic moments \mathbf{S}_j within the crystal structure, the rotational invariance in spin space can be expressed as:

$$\mathbf{B}_i^{eff}(\mathbf{S}_j) = \mathbf{R}^{-1} \mathbf{B}_i^{eff}(\mathbf{R} \mathbf{S}_j) \quad (2)$$

where \mathbf{R} is any rotation matrix. For collinear magnetic structures, one can verify that the SG construction produces a \mathbf{B}_i^{eff} with the invariance properties in eq. 2. Again, this is most easily seen using the equivalent Shubnikov approach: the Shubnikov SG is the symmetry group of the black & white antiferromagnetic ordering pattern, and is therefore independent on the direction of the Néel vector. As discussed in Ref. 3, one proceeds to construct a *scalar* field B_i^{eff} from a tensor that is fully symmetrised by the Shubnikov SG, and then equates $\mathbf{B}_i^{eff} = \hat{\mathbf{L}} B_i^{eff}$, where $\hat{\mathbf{L}}$ is a unit

vector in the direction of the Néel vector \mathbf{L} . Since in a collinear structure \mathbf{L} and the \mathbf{S}_j are all parallel/antiparallel to each other, eq. 2 is obeyed by construction. Our aim is to find an analogous treatment for $\mathbf{k}/-\mathbf{k}$ symmetric, TRO textures in *non-collinear* magnets, so that \mathbf{B}_i^{eff} is similarly invariant by construction. Note that this approach is not immediately suitable for p -wave magnets, since in this case the spin texture cannot be described as a linear combination of TRO vectors with scalar quantities, which clearly produces a TRO, parity even tensor. Moreover, in p -wave magnets, band splitting and spin polarisation are correlated, so that, for a given k , the net spin polarisation averaged over bands that would be degenerate in the absence of magnetic ordering is zero.¹⁰

III. COLOUR SYMMETRY GROUPS AND THE DESCRIPTION OF NON-COLLINEAR STRUCTURES

Colour symmetry groups are groups of combined geometrical and colour-permutational symmetry operations, which leave certain coloured objects unchanged.¹¹ In the context of crystallography, one can distinguish between colour *point* groups (CPG), where all geometrical transformations are proper and improper rotations around a fixed point, and colour *space* groups (CSG), in which rotations and translations are combined to yield the symmetries of periodic coloured objects. Within the CG framework, Shubnikov groups correspond to *bicolour* CGs. Tricolour CSGs were first classified by D. Harker in 1981,¹¹ while other authors later extended the theory to four and six colours.^{12–14} A full classification of all possible CSGs was presented by J.N. Kozev in 1988.¹⁵ Applications of CGs to physical problems were discussed as early as 1982,¹⁶ and were later extended to include the description of orbital ordering.¹⁷ Although extending the Shubnikov group analysis of magnetic structures to multicoloured groups appears quite natural, by the early eighties the representation analysis first introduced by E. F. Bertaut¹⁸ was already very popular, and the alternative CSG approach was not widely pursued.

Here, we will adopt the nomenclature first proposed by Harker to construct multi-colour groups,¹¹ in which each CSG/CPG is denoted by an ordinary space or point group, say G , followed by two of its subgroups, H and H' . H' is a subgroup of index n , where n is also the number of colours, and contains all the operations in G that leave one colour invariant, so that, for example 'red' fragments are transformed in other red fragments. Other colours are left invariant by conjugated copies of H' , which are not necessarily unique to a single colour. By contrast, H contains all the operations in G that leave *all* colours invariants. Strictly speaking, adding H to the notation is redundant, because H is the intersection of H' with all its conjugated subsets and can be readily obtained from H' and G . Note also that the colour permutation group is isomorphic to the quotient group G/H . The CPG notation used in the remainder of this paper is $\{G|H'|H\}$. Within this framework, the colour symmetry of a particular structure would consist of an ordinary point or space group operation, which only affects the position of the atoms (or fragments), composed with (o) a colour-permutation operation, which only affects the colours. So, for example if a certain geometrical operation g converts red (R) fragments to red fragments and exchanges blue (B) and green (G) fragments, the corresponding CG operation is $g \circ \{R \rightarrow R, B \rightarrow G, G \rightarrow B\}$.

When using CGs to describe magnetic structures, each direction of the magnetic moments would be represented by a distinct colour. It seems useful to consider time reversal as a special operation, (denoted as $1'$), so that structural fragments containing spins related by time reversal are represented by 'anti-colours' (e.g., red and anti-red spins would be opposite and related by time reversal). Using the notation above, $1' \equiv \{R \rightarrow \bar{R}, B \rightarrow \bar{B}, G \rightarrow \bar{G}\}$, where the bar indicates the anti-colour. An advantage of this approach is that, at any tensor rank, it is possible to represent a colour/anticolour pair with the same coloured tensor, as explained further in Sec. IV. Moreover, the notion of time reversal is preserved, as in the case of Shubnikov groups.

The exact symmetry group of the crystal + magnetic structure (MPG or magnetic space group — MSG) consists of all CPG/CSG operations for which the colour permutation corresponds to a geometrical axial vector transformation combined either with the identity or with time reversal. Hence, the MPG/MSG of a given magnetic structure is a subgroup of its CPG/CSG. By construction, magnetic structures related by a global rotation in spin space are described by the same CG, the only difference being the identification of colours with spins.

Ever since the work of E. F. Bertaut¹⁸, irreducible representations of space groups have been the primary tool to describe magnetic structures. Later, Y. A. Izyumov introduced exchange multiplets, which are sets of irreducible representations that are linked together if the magnetic Hamiltonian is invariant by rotations in spin space. There is a natural link between CGs and the theory of exchange multiplets¹⁹, which is discussed in Appendix A.

A. Colour groups and spin groups

Since each crystallographic point group (XPG) is isomorphic to a permutation group, is not surprising that a close relation exist between the CG and SG analyses of both collinear and non-collinear magnetic structures. This relation becomes transparent if one assigns a distinct colour to each arm of the star generated by the part of the SG that acts exclusively on spins, since the action of the SG on spins becomes equivalent to a colour permutation. The derivation

of all SG²⁰ is largely identical to that of CPG — for example, in Ref. 20, the groups G and H are called R and r . However, in the SG derivation, there is an extra step to associate with the quotient group R/r one of the 32 XPGs (called B in Ref. 20). It should also be noted that CG symbols encode extra information with respect to SGs. This includes not only the number of colours (i.e., of distinct spin directions), but also the specific representation of the symmetry groups that defines the transformation of all magnetic structures with the same CG symmetry (this is explained in more detail in Appendix A). In the case of SG, the same information is encoded in the orientation of the magnetic moments with respect to the symmetry operators of the group B . This will be further clarified in the examples given below.

Whether one uses CG or SG is largely a matter of preference. The CG analysis is in principle more general (it does not even require the spins to have the same magnitude), but in most practical cases this will not be significant. We find the CG approach to be somewhat more intuitive: for a generic orientation of the magnetic moments (e.g., in the presence of an applied magnetic field), the point group acting on spins are not co-aligned with those acting on atoms, and their operators do not coincide with any of the symmetry operators that are present in the paramagnetic structure. By contrast, spin (or colour) permutation has the same meaning regardless of the overall spin orientation. An example of parallel SG and CPG analyses will be given in Sec. VII B.

IV. CONSTRUCTING COLOURED ALTERMAGNETIC TENSORS

The procedure to construct altermagnetic tensors in the framework of CG theory is rather straightforward, and follows closely the case of collinear structures (bicolour groups). Using the projection method, one constructs sets of *coloured tensors* that are totally symmetric by the CPG of the magnetic structure. This is done beginning with the most generic form of a symmetric tensor of a given rank, and assigning to it a single colour (say, red). The ‘red’ tensor is then constructed by adding up all copies of the original tensor transformed in the usual way via symmetry operations in H' , where H' transforms red fragments into other red fragments, and normalising by the order of G . Likewise, the ‘blue’ tensor is obtained by adding up all copies of the original tensor transformed via $g \circ H'$, where g transforms red fragments into blue fragments, etc. The full altermagnetic tensor is then obtained as a linear combination of the coloured tensors *times* the axial unit vector corresponding to the colour assigned to the magnetic moment in the real-space structure. Once again, by construction, effective magnetic fields (i.e., spin textures) calculated using this method are invariant by eq. 2, since magnetic moments in real space and axial unit vectors in reciprocal space are parallel and hence co-rotating. Moreover, since the MPG of the magnetic structure is a *subgroup* of the CPG, it follows that the altermagnetic tensor thus constructed is always a *special case* of the general MPG tensor, which can then be decomposed into altermagnetic and residual components, precisely as in the collinear case.

The procedure to obtain coloured tensors is slightly modified in the presence of geometrical operators composed with the time reversal operator $1'$, which gives rise to anti-colours. One can obtain separate tensors for a given colour (say, red) and its anti-colour (anti-red). However, when the full altermagnetic tensor is reconstructed, the red and anti-red tensors will be multiplied by antiparallel vectors, which is equivalent to multiplying the ‘red’ vector by the *difference* of the two tensors. Using this method, one effectively halves the number of required tensors. This mirrors the procedure outlined in Ref. 3 for collinear structures, where only one TRO tensor was required rather than separate ‘black’ and ‘white’ tensors. This situation is discussed further in Sec. VI

V. $\text{Mn}_3\text{Ir}(\text{Ge},\text{Si})$

$\text{Mn}_3\text{Ir}(\text{Ge},\text{Si})$ crystallises in the crystallographic space group $P2_13$. Below the Néel temperature ($T_N=225$ K for Ge and 210 K for Si), magnetic moments on the 12 magnetic sites order forming a complex non-collinear structure with the MSG also being $P2_13$ (MPG 23).^{21,22} Spin textures and bulk properties in Mn_3IrSi were recently analysed theoretically and discussed in the context of the Landau theory.²³

In the magnetic structure refined from experimental data and also confirmed by theoretical calculations,^{21,22} all the magnetic moments on the 12 sites are non-collinear. However, groups of three moments are roughly parallel to each other and to one of the cube diagonals, the angle with the closest diagonal being $\sim 11^\circ$. The experimental magnetic structure (a) and the approximate structure (b) are displayed in Fig. 1. We begin by performing an analysis of the spin textures for the approximate structure, which requires four colours. Later, we will explain that the 12-colour analysis yields an identical result. Since the magnetic and crystallographic space groups are the same, the magnetic structure does not break any crystallographic symmetry. We therefore expect the textures arising from the 4- and 12-colour analysis to be fully consistent with the MPG textures, which are reported in Table I of Ref. 3 (MPG 23, Class XVII).

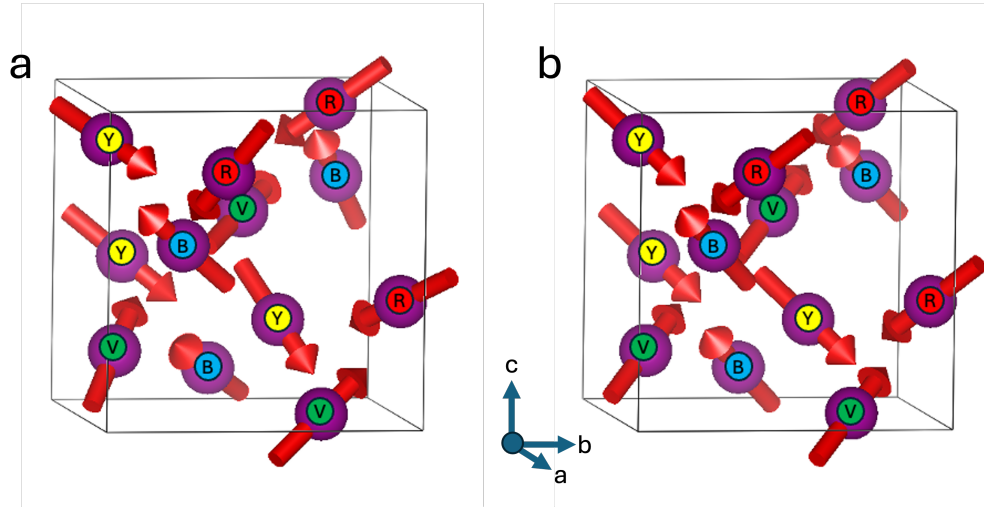


FIG. 1. (Colour online) Experimentally determined²¹ (a) and approximate (b) magnetic structures of $\text{Mn}_3\text{Ir}(\text{Ge,Si})$. Only magnetic Mn atoms are shown. Labels indicate distinct colours (see text for the assignment of magnetic moment directions to colours).

A. $\text{Mn}_3\text{Ir}(\text{Ge,Si})$: four-colour analysis

We choose the four colours to correspond to the following spin directions (see Fig. 1(b)):

$$\begin{aligned}
 \text{Yellow(Y)} &: \rightarrow (1, 1, -1) \\
 \text{Blue(B)} &: \rightarrow (1, -1, 1) \\
 \text{Green(G)} &: \rightarrow (-1, 1, 1) \\
 \text{Red(R)} &: \rightarrow (-1, -1, -1)
 \end{aligned} \tag{3}$$

The XPG (23) comprises 12 symmetry operations: 8 3-fold ($\pm 120^\circ$) rotations, around $[1, 1, 1]$ and equivalent directions, three 2-fold rotations around $[1, 0, 0]$ and equivalent directions and the identity. The MPG operations that leave Y invariant are the identity and the $\pm 120^\circ$ rotations around $[1, 1, -1]$, corresponding to point group 3. Likewise B, G, and R are left invariant by a conjugated point group, also with symbol 3 but with a different rotation axis. There are four such conjugated subgroups in the MPG 23, and the only common operation to all is the identity. Hence, the full CPG symbol is $\{23|3|1\}$. In this CPG, 3-fold rotations leave one colour invariant and permute the other three, while two-fold rotations exchange pairs of colours — for example, the two-fold rotation around $[1, 0, 0]$ exchange Y with B and G with R.

The next step is to construct four ‘coloured scalar’ tensors of the selected rank using the projection method. This is done starting from the most generic form of the symmetric scalar tensor, to which we assign the colour Y. We then apply the space transformation operations of the XPG and exchange the colours as explained in Sec. IV. We perform this operation for the lowest rank (rank 2), but the procedure is identical for any rank. The most generic rank-2 symmetric tensor is:

$$\mathcal{T}_g = \begin{pmatrix} a & d & e \\ d & b & f \\ e & f & c \end{pmatrix} \tag{4}$$

where the scalar quadratic form is obtained by multiplying this matrix to the left and right by $[k_x, k_y, k_z]$. The four coloured tensors obtained by the projection methods are:

$$\begin{aligned}
\mathcal{T}_Y &= \frac{1}{12} \begin{pmatrix} A & B & -B \\ B & A & -B \\ -B & -B & A \end{pmatrix} \\
\mathcal{T}_B &= \frac{1}{12} \begin{pmatrix} A & -B & B \\ -B & A & -B \\ B & -B & A \end{pmatrix} \\
\mathcal{T}_G &= \frac{1}{12} \begin{pmatrix} A & -B & -B \\ -B & A & B \\ -B & B & A \end{pmatrix} \\
\mathcal{T}_R &= \frac{1}{12} \begin{pmatrix} A & B & B \\ B & A & B \\ B & B & A \end{pmatrix}
\end{aligned} \tag{5}$$

with $A = a + b + c$, $B = 1/2(d - e - f)$. With this construction, the set $\{\mathcal{T}_Y, \mathcal{T}_B, \mathcal{T}_G, \mathcal{T}_R\}$ is totally symmetric by the CPG — in other words, it is invariant by all geometrical transformations composed with the colour permutation operations.

To obtain the spin texture at the lowest rank, we re-assign colours to spin texture directions (Eq. 16) and add up all the coloured tensors, obtaining the full rank-3 CPG tensor

$$\mathcal{T}_{\text{CPG}} = (1, 1, -1)\mathcal{T}_Y + (1, -1, 1)\mathcal{T}_B + (-1, 1, 1)\mathcal{T}_G + (-1, -1, -1)\mathcal{T}_R \tag{6}$$

It is apparent that the texture obtained from Eq. 6 is completely invariant by rotation in spin space in the sense of Eq. 2. The expression of \mathcal{T}_{CPG} as a 3×6 matrix is

$$\mathcal{T}_{\text{CPG}} = \begin{pmatrix} 0 & 0 & 0 & A_{14} & 0 & 0 \\ 0 & 0 & 0 & 0 & A_{14} & 0 \\ 0 & 0 & 0 & 0 & 0 & A_{14} \end{pmatrix} \tag{7}$$

with $A_{14} = 1/3(-d + e + f)$ and is formally identical to the one obtained from the MPG analysis, which is reported in Table I of Ref. 3 (MPG 23, Class XVII), exactly as we expected.

B. $\text{Mn}_3\text{Ir}(\text{Ge},\text{Si})$: 12-colour analysis

We can repeat the same analysis using the experimental magnetic structure of $\text{Mn}_3\text{Ir}(\text{Ge},\text{Si})$, which requires twelve colours, none of which is left invariant by operations other than the identity, hence the 12-colour CPG is $\{23|1|1\}$. Here, each of the four colours in the simplified magnetic structure is split into three, so that, for example:

$$\begin{aligned}
\text{Yellow1(Y1)} &: \rightarrow (v_x, v_y, v_z) \\
\text{Yellow2(Y2)} &: \rightarrow (v_y, -v_z, -v_x) \\
\text{Yellow3(Y3)} &: \rightarrow (-v_z, v_x, -v_y)
\end{aligned} \tag{8}$$

etc., where, in the experimental structure, $v_x = 0.7106$, $v_y = 1.2118$, $v_z = -1.015$. The analysis proceeds in the same way as for the 4-colour structure, yielding the same result (Eq. 7), this time with $A_{14} = 1/3(v_x f + v_y e + v_z d)$. Note the two results coincide for $\mathbf{v} = (1, 1, -1)$.

In conclusion, for $\text{Mn}_3\text{Ir}(\text{Ge},\text{Si})$, both the 4- and the 12-colour analysis produce tensorial spin textures that are fully consistent with the MPG analysis (Ref. 3), as we expected since the magnetic structure does not break any of the crystallographic symmetry operators. We generally expect this to be the case at every tensor order, whenever the ‘grey’ (paramagnetic) group corresponding to the MPG is identical to the XPG. The CPG tensorial spin texture is formally invariant by a global rotation of the magnetic structure in spin space, and this remains true for spin rotations that break one or more of the MPG 23 symmetries. If such low-symmetry magnetic structure could be stabilised, we would expect the altermagnetic component of the spin texture (given by the CPG analysis) to remain the same, while an additional component would be activated in the presence of SOC, with tensor forms consistent with the new, lower-symmetry MPG. However, to our knowledge, no such structure has been observed experimentally.

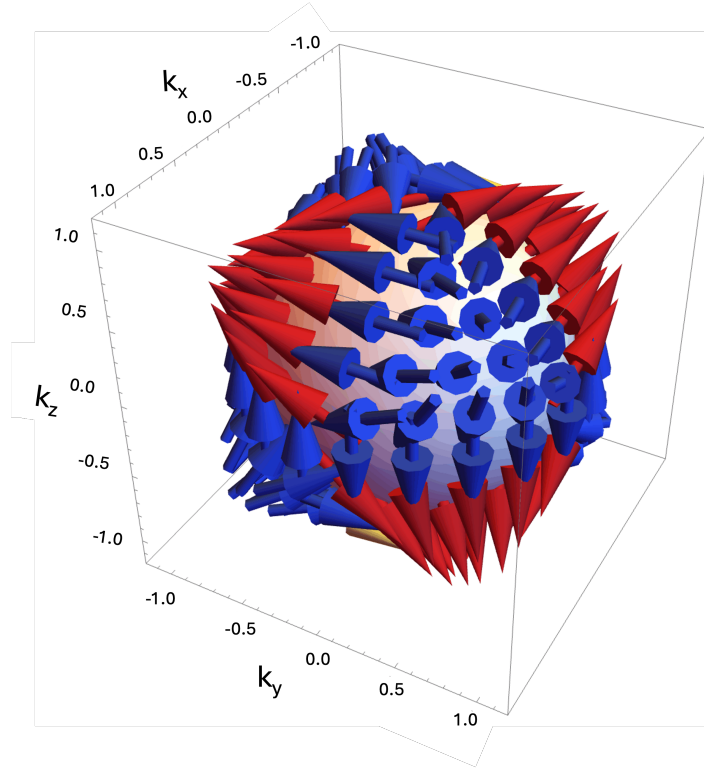


FIG. 2. (Colour online) Spin texture of Mn_3IrGa , generated from the tensor in Eq. 7. The colour of the arrows indicates the radial projection of the texture (red=out; blue=in). Wavevectors are in arbitrary units.

VI. DEALING WITH ANTI-COLOURS: THE CASE OF Pb_2MnO_4

Pb_2MnO_4 received some attention due to its potential multiferroic properties.^{24,25} It crystallises with a tetragonal structure (space group: $P\bar{4}2_1c$) and orders non-collinearly at the Γ point below ~ 18 K, with the magnetic moments on the eight Mn sites aligned along the diagonals of the square faces (Fig. 3). The MSG and MPG are $P\bar{4}'2_1c'$ and $\bar{4}'2m'$, respectively. As in the case of $\text{Mn}_3\text{Ir}(\text{Ge}, \text{Si})$, magnetic ordering does not break any crystal symmetry operator, so we expect the CPG and MPG analyses (the latter reported in in Table I, Ref. 3 as Class X) to yield identical results. However, the tensor associated with Class X has two parameters (A_{14} and A_{36}), so the specific values of these parameters in the CPG analysis will depend on the relative orientations of the spins in real space, whilst remaining invariant by global rotations in spin space.

The colours/anticolours have been associated with magnetic moment directions, as follows:

$$\begin{aligned}
 \text{Red(R)} &: \rightarrow (1, 1, 0) \\
 \text{Blue(B)} &: \rightarrow (1, -1, 0) \\
 \text{anti-Red(\bar{R})} &: \rightarrow (-1, -1, 0) \\
 \text{anti-Blue(\bar{B})} &: \rightarrow (-1, 1, 0)
 \end{aligned}$$

(9)

There are eight symmetry operators in the XPG — the identity (E), two $\bar{4}$ operations, a 2-fold rotation around z , two 2-fold axes along x and y and two mirror planes perpendicular to xy and $\bar{x}y$. The corresponding colour permutation operations are the following:

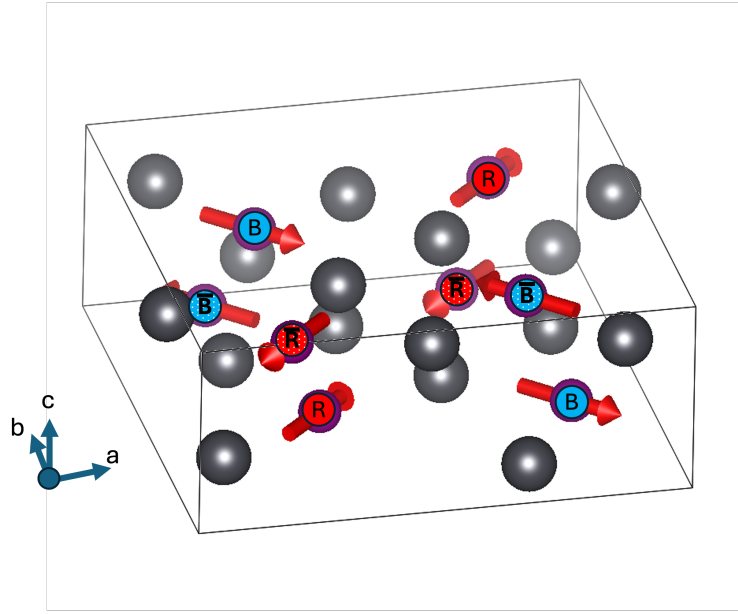


FIG. 3. (colour online) Magnetic structure of Pb_2MnO_4 , based on Ref. 24. The magnetic Mn atoms have associated arrows, while the grey spheres are Pb (oxygen atoms have been omitted). Colours and anti-colours are indicated with plain and dotted fields, respectively.

$$\begin{aligned}
 E &: R \rightarrow R; B \rightarrow B; \bar{R} \rightarrow \bar{R}; \bar{B} \rightarrow \bar{B} \\
 \bar{4}^+ &: R \rightarrow B; B \rightarrow \bar{R}; \bar{R} \rightarrow \bar{B}; \bar{B} \rightarrow R \\
 \bar{4}^- &: R \rightarrow \bar{B}; B \rightarrow R; \bar{R} \rightarrow B; \bar{B} \rightarrow \bar{R} \\
 2_z &: R \rightarrow \bar{R}; B \rightarrow \bar{B}; \bar{R} \rightarrow R; \bar{B} \rightarrow B \\
 2_x &: R \rightarrow \bar{B}; B \rightarrow \bar{R}; \bar{R} \rightarrow B; \bar{B} \rightarrow R \\
 2_y &: R \rightarrow B; B \rightarrow R; \bar{R} \rightarrow \bar{B}; \bar{B} \rightarrow \bar{R} \\
 m_{xy} &: R \rightarrow \bar{R}; B \rightarrow B; \bar{R} \rightarrow R; \bar{B} \rightarrow \bar{B} \\
 m_{\bar{xy}} &: R \rightarrow R; B \rightarrow \bar{B}; \bar{R} \rightarrow \bar{R}; \bar{B} \rightarrow B
 \end{aligned}$$

(10)

Consequently, the H' subgroup (for red and anti-red) is $m = \{E, m_{\bar{xy}}\}$, while the group H only contains the identity. The CPG symbol is $\{\bar{4}'2m'|m|1\}$. The subgroup m has index 4 in $\bar{4}'2m'$, so $\{\bar{4}'2m'|m|1\}$ is a four-colour group.

The four coloured tensors obtained by the projection methods are:

$$\begin{aligned}
 \mathcal{T}_R &= \frac{1}{8} \begin{pmatrix} A & D & B \\ D & A & B \\ B & B & C \end{pmatrix} \\
 \mathcal{T}_{\bar{R}} &= \frac{1}{8} \begin{pmatrix} A & D & -B \\ D & A & -B \\ -B & -B & C \end{pmatrix} \\
 \mathcal{T}_B &= \frac{1}{8} \begin{pmatrix} A & -D & B \\ -D & A & -B \\ B & -B & C \end{pmatrix} \\
 \mathcal{T}_{\bar{B}} &= \frac{1}{8} \begin{pmatrix} A & -D & -B \\ -D & A & B \\ -B & B & C \end{pmatrix}
 \end{aligned}$$

(11)

with $A = a + b$, $B = (ee + f)/2$, $C = 2c$, and $D = d$. We can combine each colour with its anti-colour as:

$$\begin{aligned}
\mathcal{T}_{R-\bar{R}} &= \frac{1}{4} \begin{pmatrix} 0 & 0 & B \\ 0 & 0 & B \\ B & B & 0 \end{pmatrix} \\
\mathcal{T}_{B-\bar{B}} &= \frac{1}{4} \begin{pmatrix} 0 & 0 & B \\ 0 & 0 & -B \\ B & -B & 0 \end{pmatrix}
\end{aligned} \tag{12}$$

Finally, we can reconstruct the full altermagnetic tensor using the colour assignments in eq. 9:

$$\mathcal{T}_{\text{CPG}} = \begin{pmatrix} 0 & 0 & 0 & A_{14} & 0 & 0 \\ 0 & 0 & 0 & 0 & A_{14} & 0 \\ 0 & 0 & 0 & 0 & 0 & 0 \end{pmatrix} \tag{13}$$

where $A_{14} = B$. This is to be compared with the MPG tensor for Class X:

$$\mathcal{T}_{\text{MPG}} = \begin{pmatrix} 0 & 0 & 0 & A_{14} & 0 & 0 \\ 0 & 0 & 0 & 0 & A_{14} & 0 \\ 0 & 0 & 0 & 0 & 0 & A_{36} \end{pmatrix} \tag{14}$$

so \mathcal{T}_{CPG} is a particular case of \mathcal{T}_{MPG} , while $A_{36} = 0$ clearly arises from the fact that all magnetic moments are in the xy plane. One can easily verify that \mathcal{T}_{CPG} is invariant by rotation in spin space in the sense of Eq. 2. It can also be shown that more general four-colour models based on the same CPG produce an altermagnetic tensor that is identical to \mathcal{T}_{MPG} .

VII. BREAKING CRYSTAL SYMMETRY WITH MAGNETIC MOMENTS: THE CASE OF Mn_3GaN

The cases of $\text{Mn}_3\text{Ir}(\text{Ge},\text{Si})$ and Pb_2MnO_4 were complex and instructive, but mainly served as validations of the colour symmetry approach, since there was an expectation that the results should coincide with the MPG analysis. Cases in which the crystal symmetry is explicitly broken by the magnetic structure are significantly more interesting, particularly when the phase diagram contains phases with different magnetic symmetries. The anti-perovskite family, of which Mn_3GaN is a well-known representative,^{26,27} is an ideal case in point. In the bulk, Mn_3GaN orders with a non-collinear AFM structure and $T_N \sim 290$ K, but in thin films the Néel temperature can be as high as $T_N \sim 350$ K, making this material suitable for applications in spintronics. Since the magnetic Mn sites form kagomé lattices with Ga at the empty sites, the magnetic ordering is in a typical 120° pattern, with the magnetic and crystallographic unit cells coinciding (Γ -point ordering). The crystallographic space group is $Pm\bar{3}m$ (No. 221). Two magnetic structures have been proposed for Mn_3GaN , corresponding to the Γ^{5g} and Γ^{4g} irreps of $Pm\bar{3}m$, and having MSGs $R\bar{3}m$ and $R\bar{3}m'$, respectively (see Fig. 4). Note that in both cases the cubic crystal symmetry is broken by the magnetic structure. Mn_3GaN itself appears to be ordering with Γ^{5g} in both bulk²⁶ and thin film²⁸ forms, but DFT calculations²⁹ have shown that Γ^{4g} can be stable for other members of the antiperovskite family, sometimes associated with a Γ^{5g}/Γ^{4g} phase transition. As drawn in Fig. 4, the magnetic moments in the two structures are related by a 90° collective rotation of the magnetic moments in spin space. However, the MPG $\bar{3}m'$ of the Γ^{4g} is *admissible*, i.e., it allows the development of SOC-induced weak ferromagnetism via collective tilting of the moments towards the $[1, 1, 1]$ direction.

A. Mn_3GaN : CPG analysis

The XPG $m\bar{3}m$ comprises 48 symmetry operations, but improper operations have the same effect on magnetic moments as the corresponding proper rotations, so it will be sufficient to consider the 24 operations of point group 432: eight 3-fold ($\pm 120^\circ$) rotations, around $[1, 1, 1]$ and equivalent directions, three 2-fold rotations and six 4-fold rotations around $[1, 0, 0]$ and equivalent, six 2-fold rotations around $[1, 1, 0]$ equivalent, and the identity. The colour assignment (shown in Fig. 4) is the same for the Γ^{5g} and Γ^{4g} structures, except for a collective rotation in spin space. For Γ^{5g} :

$$\begin{aligned}
R^{5g} &: \rightarrow \frac{1}{\sqrt{2}} (0, 1, -1) \\
B^{5g} &: \rightarrow \frac{1}{\sqrt{2}} (1, -1, 0) \\
G^{5g} &: \rightarrow \frac{1}{\sqrt{2}} (-1, 0, 1)
\end{aligned} \tag{15}$$

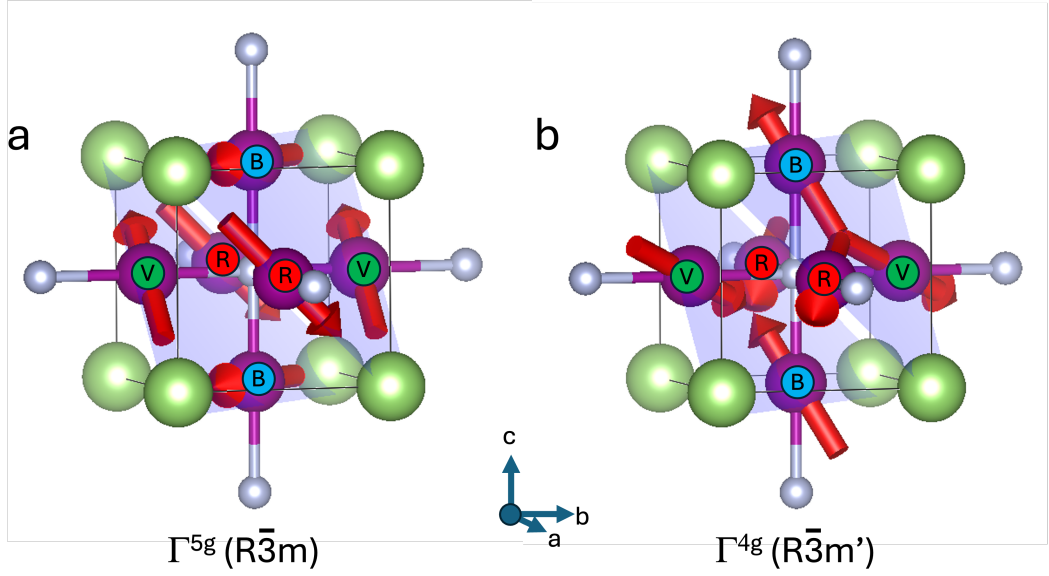


FIG. 4. Magnetic structures of the Γ^{5g} (a) and Γ^{4g} (b) phases of Mn_3GaN .²⁶ Magnetic Mn ions are shown with arrows, small spheres are N and large spheres are Ga. (111) planes containing the Mn kagomé lattice are shadowed.

while for Γ^{4g} :

$$\begin{aligned}
 \mathbf{R}^{4g} &: \rightarrow \frac{1}{\sqrt{6}} (-2, 1, 1) \\
 \mathbf{B}^{4g} &: \rightarrow \frac{1}{\sqrt{6}} (1, 1, -2) \\
 \mathbf{G}^{4g} &: \rightarrow \frac{1}{\sqrt{6}} (1, -2, 1)
 \end{aligned} \tag{16}$$

By inspection, the three-fold rotations permute the three colours, the $[1, 0, 0]$ -2-fold rotations leave all colours invariant, whilst the $[1, 0, 0]$ -4-fold rotations and $[1, 1, 0]$ -2-fold rotations leave one colour invariant and permute the other two. Hence, the colour group symbol is $\{432|422|222\}$. The point group 422 is a subgroup of index three, so $\{432|422|222\}$ is indeed a three-colour group.

Next, we construct the coloured tensors with the projection method, starting from a generic rank-2 tensor (Eq. 4) and, this time, assigning the colour red (R) to it:

$$\begin{aligned}
 \mathcal{T}_R &= \frac{1}{6} \begin{pmatrix} 2a & 0 & 0 \\ 0 & b+c & 0 \\ 0 & 0 & b+c \end{pmatrix} \\
 \mathcal{T}_B &= \frac{1}{6} \begin{pmatrix} b+c & 0 & 0 \\ 0 & b+c & 0 \\ 0 & 0 & 2a \end{pmatrix} \\
 \mathcal{T}_G &= \frac{1}{6} \begin{pmatrix} b+c & 0 & 0 \\ 0 & 2a & 0 \\ 0 & 0 & b+c \end{pmatrix}
 \end{aligned}$$

Re-assembling the full CPG tensor we obtain for Γ^{5g} :

$$\mathcal{T}_{\text{CPG}}^{5g} = \Lambda \begin{pmatrix} 0 & 1 & -1 & 0 & 0 & 0 \\ -1 & 0 & 1 & 0 & 0 & 0 \\ 1 & -1 & 0 & 0 & 0 & 0 \end{pmatrix} \tag{17}$$

with $\Lambda = -(1/(6\sqrt{2}))(2a - b - c)$, while for Γ^{4g} :

$$\mathcal{T}_{\text{CPG}}^{4g} = \Lambda \begin{pmatrix} 2 & -1 & -1 & 0 & 0 & 0 \\ -1 & 2 & -1 & 0 & 0 & 0 \\ -1 & -1 & 2 & 0 & 0 & 0 \end{pmatrix} \tag{18}$$

with $\Lambda = -(1/(6\sqrt{6}))(2a - b - c)$

The two tensor are orthogonal, meaning that the spin textures will be orthogonal at any wavevector.

As already explained, the MPGs for the Γ^{5g} and Γ^{4g} ($\bar{3}m$ and $\bar{3}m'$, Class VIII and Class VII, respectively in Table I of Ref. 3) belong to the trigonal system. Therefore, in order to compare them to the CPG tensors, we need to rotate them to the cubic coordinates. The simple transformations yield:

$$\mathcal{T}^{\bar{3}m} = \Lambda_1 \begin{pmatrix} 0 & 1 & -1 & 0 & 0 & 0 \\ -1 & 0 & 1 & 0 & 0 & 0 \\ 1 & -1 & 0 & 0 & 0 & 0 \end{pmatrix} + \Lambda_2 \begin{pmatrix} 0 & 0 & 0 & 0 & 1 & -1 \\ 0 & 0 & 0 & -1 & 0 & 1 \\ 0 & 0 & 0 & 1 & -1 & 0 \end{pmatrix} \quad (19)$$

$$\mathcal{T}^{\bar{3}m'} = \Lambda_1 \begin{pmatrix} 2 & -1 & -1 & 0 & 0 & 0 \\ -1 & 2 & -1 & 0 & 0 & 0 \\ -1 & -1 & 2 & 0 & 0 & 0 \end{pmatrix} + \Lambda_2 \begin{pmatrix} 0 & 0 & 0 & 2 & -1 & -1 \\ 0 & 0 & 0 & -1 & 2 & -1 \\ 0 & 0 & 0 & -1 & -1 & 2 \end{pmatrix} + \Lambda_3 \begin{pmatrix} 1 & 1 & 1 & 0 & 0 & 0 \\ 1 & 1 & 1 & 0 & 0 & 0 \\ 1 & 1 & 1 & 0 & 0 & 0 \end{pmatrix} \quad (20)$$

One can easily see that $\mathcal{T}_{\text{CPG}}^{5g}$ (Eq. 17) is equal to the first term of $\mathcal{T}^{\bar{3}m}$ (Eq. 19) with $\Lambda \rightarrow \Lambda_1$. Likewise, $\mathcal{T}_{\text{CPG}}^{4g}$ (Eq. 18) is equal to the first term of $\mathcal{T}^{\bar{3}m'}$ (Eq. 20) with $\Lambda \rightarrow \Lambda_1$. In other words, tensors obtained from the CPG analysis are *special cases* of the general tensors allowed by the MPG, obtained, in this case by setting $\Lambda_2 = \Lambda_3 = 0$. This is exactly what we expected and is completely consistent with the result we previously obtained for collinear structures (Ref. 3).

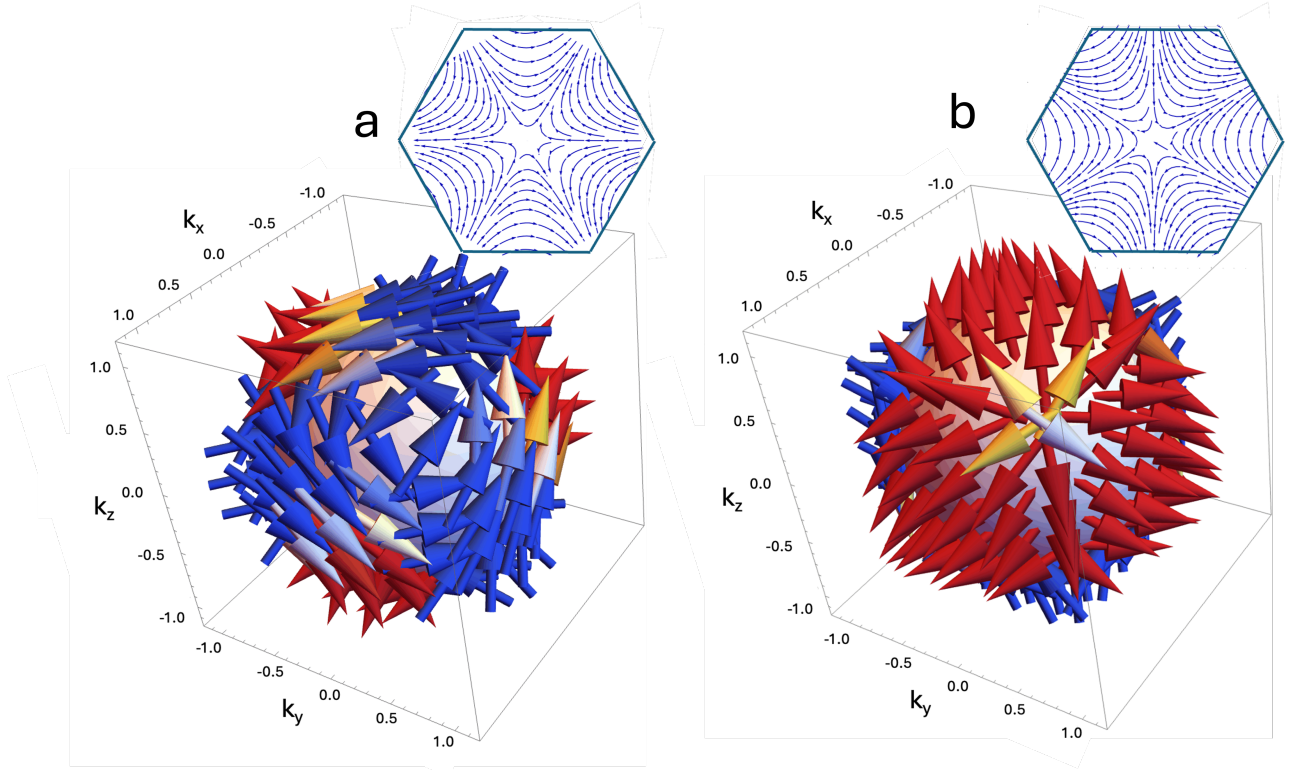


FIG. 5. (Colour online) Altermagnetic spin textures for the Γ^{5g} (a) Γ^{4g} (b) and phases of Mn_3GaN , generated from the tensors $\mathcal{T}_{\text{CPG}}^{5g}$ and $\mathcal{T}_{\text{CPG}}^{4g}$ (Eqs. 17 and 18). The colour of the arrows indicates the radial projection of the texture (red=out; yellow/grey=parallel; blue=in). Wavevectors are in arbitrary units. The insets are the equatorial cross sections of the textures down the (1,1,1) direction, shown with an outline of the Brillouin zone (compare with Fig. 6). The Γ^{5g} and Γ^{4g} texture are related by a collective 90° -rotation in spin space around the (1,1,1) direction.

B. Mn_3GaN and $\text{Mn}_3\text{Ir}(\text{Ge},\text{Si})$: SG analysis

Here, we give examples of analyses performed on Mn_3GaN and $\text{Mn}_3\text{Ir}(\text{Ge},\text{Si})$ with the SG approach and using the terminology and numbering of Ref. 20. As already mentioned, the SGs corresponding to a given CPG are obtained

from the XPG $G(R)$ and one of its normal subgroups $H(r)$, where the letter in brackets corresponds to the notation of Ref. 20.

In the case of Mn_3GaN , $G = 432$ and $H = 222$. The spin group is constructed by selecting spin-transformation PGs (denoted as B) that are isomorphic to G/H (or R/r in the notation of Ref. 20). There are two possible PGs for B : 32 (SG no. 563) and $3m$ (SG no. 564), which are, indeed, both isomorphic to the three-colour permutation group. In Ref. 20, it is explained that the two coordinate systems for G and B are arbitrarily mutually orientated, though a complex notation is introduced when the coordinate systems of B and G do not coincide. However, importantly, one needs to orient the axes of B so that they act correctly on the spin system in real space. In our case, the three-fold axis must be perpendicular to the three spins, each two-fold axis in 32 must be parallel to one of the spins, and each mirror plane in $3m$ must be perpendicular to one of the spins. When this is done, the analysis is identical to the one using CPGs, since B acts by permuting the spins in the same way as colours were permuted by the CPG. Note, however, the B needs to be rotated by 90° rotation between Γ^{5g} and Γ^{4g} and more generally re-oriented to fit an arbitrary rotation in spin space. Leaving aside the $32/3m$ ambiguity, this seems an unnecessary complication that is completely avoided by the CPG analysis. Within the tensorial framework, the CPG analysis also captures the fundamentally *scalar* nature of altermagnetic tensors.

Similarly, a parallel SG analysis can be performed on $\text{Mn}_3\text{Ir}(\text{Ge},\text{Si})$, where $G = 23$ and $H = 1$ (SG 538 in Ref. 20). Here, the SG is the *same* for the approximate and experimental magnetic structures (see Sec. V and VB), while the CPG are different — $\{23|3|1\}$ vs $\{23|1|1\}$ because, as already explained, the CPG symbol encode additional information about the number of colours (i.e., distinct spin directions) and the specific representation that encodes the colour permutation.

C. Mn_3GaN : DFT calculations

To validate our analysis further, we calculated the spin textures for the Γ^{5g} and Γ^{4g} phases of Mn_3GaN using spin-resolved DFT. DFT calculations were performed using the Quantum-ESPRESSO code³⁰. The exchange and correlation effects were treated within the generalized gradient approximation (GGA)³¹. The k-point mesh of $16 \times 16 \times 16$ and plane-wave cut-off energy of 52 Ry were used for the integration in the irreducible Brillouin zone. The non-collinear magnetic structure was always considered with and without spin orbit coupling. The spin texture on the Fermi surface was calculated using $50 \times 50 \times 50$ k points within the first Brillouin zone (BZ). To depict the results in an intuitive manner, the spin texture was projected on a plane containing the Γ point and normal to the $(1, 1, 1)$ direction.

In order to compare these with the textures obtained with the CPG analysis, one should keep in mind the following aspects:

1. The full DFT spin texture will require a tensor expansion to higher orders, while for simplicity our CPG analysis was limited to rank-3 (i.e., with coloured tensors of rank 2).
2. With DFT, the spin texture is calculated on constant-energy surfaces rather than at constant $|\mathbf{k}|$. However, since constant-energy surfaces have at least the full symmetry of the XPG, textures will have an identical tensorial expansion, though the coefficients will be different.

Fig. 6 display sections of the spin-resolved Fermi surface, calculated for Γ^{5g} and Γ^{4g} with and without SOC. For Γ^{4g} , the colour wheel indicating in-plane spin directions was rotated by 90° , to emphasise the expected relation with the Γ^{5g} texture. In the absence of SOC, the Γ^{5g} (panel a) and Γ^{4g} (panel c) are identical except for the 90° rotation, and there is no spin-texture component along $(1, 1, 1)$, as predicted by the CPG analysis. The spin textures are also very similar to those in Fig. 5 (see insets for the same cuts), though the DFT textures have more complexity arising from higher-rank tensorial components. By contrast, in the presence of SOC, the Γ^{5g} (panel b) and Γ^{4g} (panel d) become significantly different, and Γ^{4g} acquires a component along $(1, 1, 1)$, exactly as expected.

VIII. DISCUSSION AND CONCLUSIONS

In this paper, ‘altermagnetic textures’ have been defined as the components of the momentum-space spin texture that is invariant by global rotations in spin space in the sense of Eq. 2. The tensorial forms of these textures can be defined consistently based on CPG analysis for both non-collinear and collinear AFM structures, since the latter are a special example of bi-colour (black and white) symmetry. Strong FM textures (i.e., those present in a true ferro/ferrimagnet rather than a weak/canted FM) are also a special example, for which the colour group is trivial (colourless). In addition to altermagnetic textures, the MPG of the crystal/magnetic structure will generally allow additional spin textures in momentum space, which will be specific to a given orientation of the spin system and will

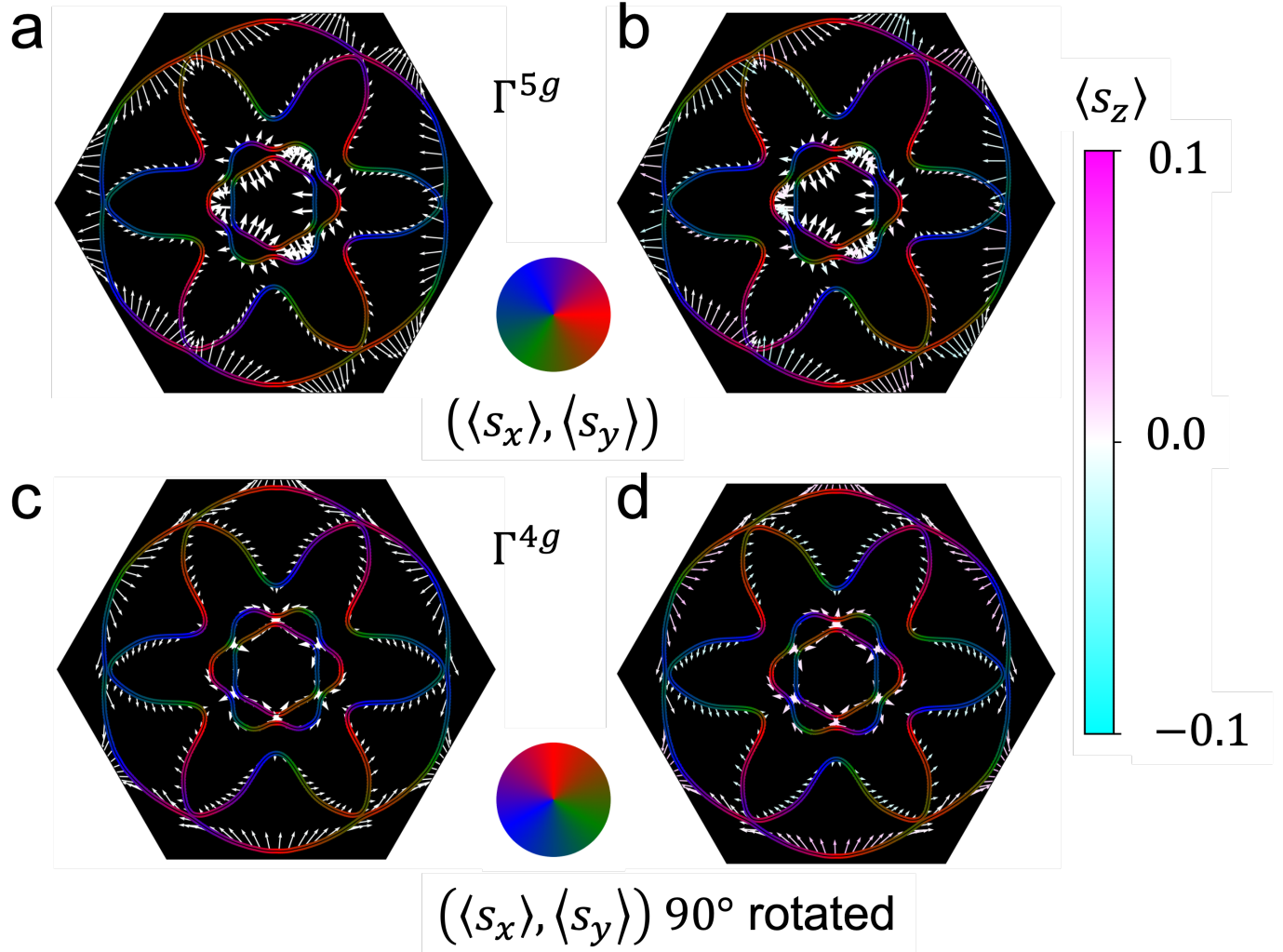


FIG. 6. (Colour online) Spin texture at the Fermi surface on a plane cut perpendicular to the $(1, 1, 1)$ direction including the Γ point shown with an outline of the BZ, calculated using spin-resolved DFT for the Γ^{5g} (top) and Γ^{4g} (bottom) phases with (a, c) and without (b,d) SOC. For Γ^{4g} , the colour wheel indicating in-plane spin directions was rotated by 90° . The z -component, which is only present for Γ^{4g} with SOC, is also indicated. The z direction is along $(1, 1, 1)$.

be absent in the absence of SOC. Altermagnetic/ferromagnetic textures are allowed at some tensorial order for all MPGs that do not explicitly forbid $\mathbf{k}/-\mathbf{k}$ symmetric, time-reversal odd spin textures (i.e., those that do not contain the time reversal operator or the product of inversion and time reversal operators). The MPG/CPG pair defines which part of the full MPG texture (tabulated to lowest tensorial order in Ref. 3) is altermagnetic, with the CPG also providing the ‘tensorial building blocks’ (coloured tensors) to reconstruct the full altermagnetic texture, once the exact real-space spin orientations are defined. These building blocks can in principle be derived for all CPGs once and for all, though calculating them for a specific magnetic structure is a simple exercise. We have demonstrated the CPG approach for three non-collinear magnetic structures — $\text{Mn}_3\text{Ir}(\text{Ge},\text{Si})$, Pb_2MnO_4 and Mn_3GaN . In the case of Mn_3GaN , using DFT we have also calculated the spin textures for two different magnetic phases (Γ^{5g} and Γ^{4g}) with and without SOC, and demonstrated that they are entirely consistent with the predictions of MPG/CPG theory.

Beyond the results reported in this paper, we remark that CPG/CSG symmetry can also be defined for p -wave magnets, which allow $\mathbf{k}/-\mathbf{k}$ anti-symmetric, time-reversal even spin textures in momentum space, and it is expected that those spin textures will also be constrained by CSG symmetry. However, our tensorial analysis cannot be straightforwardly employed, and a new theory will need to be developed to deal with such systems.

Appendix A: Colour symmetry, representations and exchange multiplets

There is a close relation between the description of magnetic structures in terms of CGs and the theory of exchange multiplets,¹⁹ which classifies magnetic structures in terms of irreducible representations (*irreps*) of the symmetry group of a Hamiltonian that only involves symmetric exchange and is therefore invariant by rotation in spin space. The symmetry of this Hamiltonian is higher than the crystal symmetry, thus, in general, several *irreps* of the space group will be combined into so-called ‘exchange multiplets’, and may be activated simultaneously at a magnetic phase transition. Exchange multiplets are constructed as tensor products of a *single irrep* of the space group that is contained in the full permutational (scalar) representation of the equivalent magnetic sites (with dimensionality equal to the number of sites), times the (generally reducible) axial-vector representation (see Ref. 19).

By contrast, the set of all possible magnetic structures with a given CG and for a given set of equivalent magnetic sites is constructed as the tensor product of the ‘colour-permuting representation’ times the axial-vector representation. In turn, the colour-permuting representation is the permutational representation of the magnetic sites restricted to the subspace defined by a one-colour basis set, where all the sites with a given colour are assigned the number ‘1’, while all the other sites are assigned ‘0’. This basis set can be easily constructed projectively from the one-site basis of the permutational representation. This is done from the left-coset decomposition of H' in G :

$$G = H' + g_1 \circ H' + g_2 \circ H' + \dots \quad (\text{A1})$$

Let \mathbf{b} be an element of the one-site basis set of the permutational representation of the magnetic sites, such that one of the sites is associated with the number ‘1’ and all the others with ‘0’. Let h'_i , $i = 1 \dots n$ be all the elements of H' . Then the elements of the one-colour basis set, say \mathbf{b}_R , \mathbf{b}_Y , \mathbf{b}_G , etc., are defined as

$$\begin{aligned} \mathbf{b}_R &= \frac{1}{n} \sum_{i=1}^n h'_i[\mathbf{b}] \\ \mathbf{b}_Y &= \frac{1}{n} \sum_{i=1}^n g_1 \circ h'_i[\mathbf{b}] \\ \mathbf{b}_G &= \frac{1}{n} \sum_{i=1}^n g_2 \circ h'_i[\mathbf{b}] \\ &\dots \end{aligned} \quad (\text{A2})$$

One can easily see that this basis is in accord with the definition of the CGs, whereby ‘red’ sites are those where \mathbf{b}_R is non-zero, etc. H' brings red sites into red sites, $g_1 \circ H'$ brings red sites into yellow sites, etc. The CG also defines the representation of G onto the linear space defined by the one-colour basis set, since the transformation matrices can be written out explicitly.

A basis set for the linear space of all magnetic structures with a given colour group is:

$$\left(\mathbf{b}_R \hat{\mathbf{i}}, \mathbf{b}_R \hat{\mathbf{j}}, \mathbf{b}_R \hat{\mathbf{k}}, \mathbf{b}_Y \hat{\mathbf{i}}, \mathbf{b}_Y \hat{\mathbf{j}}, \mathbf{b}_Y \hat{\mathbf{k}}, \mathbf{b}_G \hat{\mathbf{i}}, \mathbf{b}_G \hat{\mathbf{j}}, \mathbf{b}_G \hat{\mathbf{k}}, \dots \right) \quad (\text{A3})$$

A generic elements of this linear space is:

$$\mathbf{b}_R \mathbf{v}_1 + \mathbf{b}_Y \mathbf{v}_2 + \mathbf{b}_G \mathbf{v}_3 + \dots \quad (\text{A4})$$

where \mathbf{v}_1 , \mathbf{v}_2 , etc. are generic linear combinations of the unit vectors $\hat{\mathbf{i}}$, $\hat{\mathbf{j}}$ and $\hat{\mathbf{k}}$. This corresponds to assign a generic vector to each of the colours, exactly as we anticipated.

Finally, since the colour-permuting representation, with dimensionality equal to the number of colours, is generally *reducible*, it follows that each CG describes several exchange multiplets.

* Corresponding author: p.g.radaelli@physics.ox.ac.uk

† Corresponding author: gautam.gurung@trinity.ox.ac.uk

¹ L. Šmejkal, J. Sinova, and T. Jungwirth, *Physical Review X* **12**, 031042 (2022).

- ² L. Šmejkal, J. Sinova, and T. Jungwirth, *Physical Review X* **12**, 040501 (2022), [arXiv:2204.10844](#).
- ³ P. G. Radaelli, *Physical Review B* **110**, 214428 (2024).
- ⁴ A. B. Hellenes, T. Jungwirth, R. Jaeschke-Ubierno, A. Chakraborty, J. Sinova, and L. Šmejkal, (2023), [arXiv:2309.01607](#).
- ⁵ G. Dresselhaus, *Physical Review* **100**, 580 (1955).
- ⁶ E. I. Rashba and V. Sheka, *Fiz. Tverd. Tela: Collected Papers* **2**, 62 (1959).
- ⁷ J. Železný, Y. Zhang, C. Felser, and B. Yan, *Physical Review Letters* **119**, 187204 (2017), [arXiv:1702.00295](#).
- ⁸ J. Sticht, K. H. Höck, and J. Kübler, *Journal of Physics: Condensed Matter* **1**, 8155 (1989).
- ⁹ As explained in the remainder, the CG approach can be employed to describe the magnetic structures of p -wave magnets, but coloured tensors as defined here are not immediately useful. For this reason, we will exclude p -wave magnets from our treatment.
- ¹⁰ B. Brekke, P. Sukhachov, H. G. Giil, A. Brataas, and J. Linder, (2024), [arXiv:2405.15823](#).
- ¹¹ D. Harker, *Acta Crystallographica Section A* **37**, 286 (1981).
- ¹² J. Sivadrière, *Acta Crystallographica Section A* **40**, 573 (1984).
- ¹³ R. L. Roth, *Acta Crystallographica Section A* **41**, 484 (1985).
- ¹⁴ J. Sivadrière, *Acta Crystallographica* **44**, 735 (1988).
- ¹⁵ J. N. Kotzev and D. A. Alexandrova, *Acta Crystallographica Section A* **44**, 1082 (1988).
- ¹⁶ D. B. Litvin, J. N. Kotzev, and J. L. Birman, *Physical Review B* **26**, 6947 (1982).
- ¹⁷ Z. Jiráček, *Physical Review B* **46**, 8725 (1992).
- ¹⁸ E. F. Bertaut, *Acta Crystallographica Section A* **24**, 217 (1968).
- ¹⁹ Y. A. Izyumov, *Journal of Magnetism and Magnetic Materials* **15-18**, 497 (1980).
- ²⁰ D. B. Litvin, *Acta Crystallographica Section A* **33**, 279 (1977).
- ²¹ T. Eriksson, L. Bergqvist, P. Nordblad, O. Eriksson, and Y. Andersson, *Journal of Solid State Chemistry* **177**, 4058 (2004).
- ²² T. Eriksson, R. Lizárraga, S. Felton, L. Bergqvist, Y. Andersson, P. Nordblad, and O. Eriksson, *Physical Review B* **69**, 054422 (2004).
- ²³ M. Hu, O. Janson, C. Felser, P. McClarty, J. van den Brink, and M. G. Vergniory, (2024), [arXiv:2410.17993](#).
- ²⁴ S. A. Kimber and J. P. Attfield, *Journal of Materials Chemistry* **17**, 4885 (2007).
- ²⁵ D. C. Kakarla, H. C. Wu, D. J. Hsieh, P. J. Sun, G. J. Dai, J. Y. Lin, J. L. Her, Y. H. Matsuda, L. Z. Deng, M. Gooch, C. W. Chu, and H. D. Yang, *Physical Review B* **99**, 195129 (2019).
- ²⁶ E. F. Bertaut, D. Fruchart, J. P. Bouchaud, and R. Fruchart, *Solid State Communications* **6**, 251 (1968).
- ²⁷ K. Shi, Y. Sun, J. Yan, S. Deng, L. Wang, H. Wu, P. Hu, H. Lu, M. I. Malik, Q. Huang, and C. Wang, *Advanced materials (Deerfield Beach, Fla.)* **28**, 3761 (2016).
- ²⁸ T. Nan, C. X. Quintela, J. Irwin, G. Gurung, D. F. Shao, J. Gibbons, N. Campbell, K. Song, S. Y. Choi, L. Guo, R. D. Johnson, P. Manuel, R. V. Chopdekar, I. Hallsteinsen, T. Tybell, P. J. Ryan, J. W. Kim, Y. Choi, P. G. Radaelli, D. C. Ralph, E. Y. Tsybal, M. S. Rzechowski, and C. B. Eom, *Nature Communications* **2020 11:1** **11**, 1 (2020), [arXiv:1912.12586](#).
- ²⁹ H. K. Singh, I. Samathrakris, N. M. Fortunato, J. Zemen, C. Shen, O. Gutfleisch, and H. Zhang, *npj Computational Materials* **2021 7:1** **7**, 1 (2021), [arXiv:2009.06440](#).
- ³⁰ P. Giannozzi, O. Andreussi, T. Brumme, O. Bunau, M. Buongiorno Nardelli, M. Calandra, R. Car, C. Cavazzoni, D. Ceresoli, M. Cococcioni, N. Colonna, I. Carnimeo, A. Dal Corso, S. De Gironcoli, P. Delugas, R. A. Distasio, A. Ferretti, A. Floris, G. Fratesi, G. Fugallo, R. Gebauer, U. Gerstmann, F. Giustino, T. Gorni, J. Jia, M. Kawamura, H. Y. Ko, A. Kokalj, E. Küçükbenli, M. Lazzeri, M. Marsili, N. Marzari, F. Mauri, N. L. Nguyen, H. V. Nguyen, A. Otero-De-La-Roza, L. Paulatto, S. Poncé, D. Rocca, R. Sabatini, B. Santra, M. Schlipf, A. P. Seitsonen, A. Smogunov, I. Timrov, T. Thonhauser, P. Umari, N. Vast, X. Wu, and S. Baroni, *Journal of Physics: Condensed Matter* **29**, 465901 (2017), [arXiv:1709.10010](#).
- ³¹ J. P. Perdew, K. Burke, and M. Ernzerhof, *Phys. Rev. Lett.* **77**, 3865 (1996).